Design of Replicated Open-Pore Aluminium Cellular Materials with a Non-Stochastic Structure for Sound Absorption Applications

J. Carbajo[1] · J. M. Molina[2] · S. Kim[3,4] · L. P. Maiorano[2] · S. Ghaffari Mosanenzadeh[4] · N. X. Fang[4]

Abstract

Several porous materials, especially natural fibres and polyurethane foams, are frequently used as sound absorbers in multiple noise reduction applications. Notwithstanding their excellent absorption performance, these materials usually lack the structural strength and fire resistance required for use in aggressive environments or situations requiring structural stability. This paper proposes the design of open-pore polymer and aluminum cellular materials with non-stochastic structures for sound absorption. These materials were fabricated using additive manufacturing (polymeric materials) and the replication method (aluminum materials), which involves infiltrating porous preforms formed by compacting spheres of a martyr material, such as NaCl, with liquid aluminum. The proposed materials can be employed as a resonator system when backed by an air cavity, with the change in cavity depth used to tune its sound absorption peak. Following the standard ASTM E1050, the sound absorption of these materials was investigated. In addition, the sound absorption performance of the materials was predicted using an Equivalent Circuit Method model. The experimental results are consistent with those predicted by the model, highlighting the potential of the microstructural and configurational design of these materials as sound absorbers.

✉ J. Carbajo
  jesus.carbajo@ua.es

  J. M. Molina
  jmmj@ua.es

  S. Kim
  kimseok@changwon.ac.kr; kimseok@mit.edu

  L. P. Maiorano
  lucila.maiorano@ua.es

  S. Ghaffari Mosanenzadeh
  mosanen@mit.edu

  N. X. Fang
  nicfang@mit.edu

1   Department of Physics, Systems Engineering and Signal Theory, University of Alicante, San Vicente del Raspeig, Spain

2   University Materials Institute of Alicante, University of Alicante, San Vicente del Raspeig, Spain

3   Department of Mechanical Engineering, Changwon National University, Changwon, South Korea

4   Department of Mechanical Engineering, Massachusetts Institute of Technology, Cambridge, Massachusetts, USA

1 Introduction

Sound absorption has become a challenge that conditions the progress of many technological applications due to its direct impact on people's health and quality of life [1]. Persistent efforts to achieve adequate sound absorption have led to the development of new materials, structures, and objects that can convert sound energy into other forms of energy, most commonly heat. For sound absorption, porous materials such as fibreglass, Kevlar, polyesters, polyurethane, and open-cell porous metallic structures are frequently utilized [1–3].

Porous metallic materials with an open cell structure combine one or more solid phases with a gas phase. While the gas phase is capable of transporting sound energy into the material, the solid phase normally acts as an acoustic barrier (i. e. a motionless skeleton) and may also provide structural stability, thermal conductivity, electrical conductivity, or magnetic shielding. This combination of properties demonstrates that cellular metallic materials are suitable for applications requiring maximum sound absorption, relatively low weight, a high Young's modulus, low moisture absorption, and strong fire resistance [3, 4]. Traditional metallic cellular materials manufactured using a variety of foaming

techniques have microstructures with variable sound absorption properties. Typical absorbent cellular materials have bottleneck structures, permeabilities, and porosities in the range of 0.4–1.5×10^{-9} m^2 and 60%–80%, respectively, and single-sized pores [5]. Several works can be found in the literature dealing with the study of the acoustic properties of metallic foams from a microstructural approach [6–9]. As an acoustic wave propagates through these microstructures, the primary visco-elastic dissipation mechanisms are viscous friction losses generated in the interconnection windows between pores and thermal losses on the pore walls. Despite these advantages, due to their stochastic microstructure, their pore sizes, porosity, and wall thicknesses are all regulated over a relatively wide range, making it difficult to tune their sound absorption to a specific frequency.

In this regard, advancements have been made in open-cell cellular materials with additively manufactured periodic structural patterns [10]. Many works can be found in the literature ranging from the design of an ultra-thin metamaterial panel for perfect sound absorption [11] to a hollow core sandwich structure with tuned vibration insulation properties [12]. In this context, a metamaterial consisting of a network of interconnected resonant cavities is a microstructural design that has aroused significant attention in recent years. Cheng et al. [13] demonstrated the capabilities of such a metamaterial through both a theoretical approach and experiments involving metallic sound absorbers fabricated by selective laser melting. Similar work was carried out by Kennedy et al. [14] to study its acoustic behaviour through numerical modeling and experimental validation using three different polymer-based printing technologies. Recently, Seçgin and Baygün [15] determined the effective medium parameters of these metamaterials using an inverse method, and Sailesh et al. [16] analysed the effect of using spheres of various sizes on the sound absorption performance of 3D printed biodegradable materials. Even though these valuable works demonstrated the potential of such structures as sound absorbers, there are still some issues that deserve further study, such as their applicability in severe environments where polymer-based technologies may not be appropriate (eg. high-temperature or high-speed flow scenarios).

This work demonstrates the capacity of traditional replication processing to generate periodic structures in aluminium cellular materials. The manufacturing of sound-absorbent materials with a metal matrix is also a great challenge and frequently requires expensive production techniques. These materials have several advantages over previous materials. On the one hand, they have multiple levels of control over their microstructures, including pore size and distribution as well as window size and distribution, which enables them to be tailored to induce absorption at specified frequencies. On the other hand, their replication-based fabrication approach makes them particularly attractive for applications requiring vast quantities of material. As for their use in aggressive scenarios, their higher durability and resistance to environmental agents make these materials a great choice in terms of sustainability for the sake of environmental preservation. Several polymeric and metallic cellular specimens were fabricated using additive manufacturing techniques on polyacrylate-based resin and the replication method on high-purity aluminium, respectively. Impedance tube experiments were carried out to assess the sound absorption performance of these materials following the ASTM E1050 standard. In addition, a prediction model based on the Equivalent Circuit Method (ECM) was implemented, with results for sound absorption agreeing well with those obtained experimentally. The derived model was also used to conduct a parametric study as a function of the microstructural characteristics of the cellular materials, which may be of great utility in the design of these materials for optimal sound absorption performance.

2 Background Theory

2.1 Basic Theory of Sound Absorbers: The Acoustic Resonator

A sound absorber may be considered any device or system which attenuates sound energy when an acoustic wave propagates through it. Among these, porous absorbers such as fibrous media, foams, and perforated panels, are extensively used in many noise reduction applications. The main loss mechanisms in air-saturated porous media are attributed to viscous friction and thermal conduction in its pore network [17], being the sound absorption features determined by its microstructure. When a porous material is backed by an air cavity and a rigid wall an acoustic resonator system can be achieved. In this case, the effective sound absorption bandwidth of the resonator can be tuned, its resonance frequency determined by the air cavity depth. To assess the sound absorption performance of an acoustic resonator under plane wave incidence it is necessary to determine the surface impedance of the whole system either theoretically or from experiments in an impedance tube. Once the surface impedance of the resonator system is obtained, it is straightforward to derive its sound absorption coefficient α as

$$\alpha = 1 - \left| \frac{Z_s - Z_0}{Z_s + Z_0} \right|^2 \tag{1}$$

where Z_S is the frequency-dependent complex surface impedance of the resonator system, and $Z_0 = \rho_0 c_0$ is the characteristic impedance in air, being ρ_0 the air density, and c_0 the sound speed in air.

In general, the surface impedance of an acoustic resonator can be theoretically determined from the acoustic properties of its components (i. e. the porous layer and the air cavity). Several approaches exist to predict the acoustic properties of porous media whose pore size is much smaller than the wavelength of the acoustic wave propagating through it, being the most extensively used fluid-equivalent theory [17] and the Equivalent Circuit Method (ECM) [18].

2.2 Modeling of Acoustic Resonators Using the Equivalent Circuit Method (ECM)

The Equivalent Circuit Method (ECM) is commonly used to analyse the acoustic performance of a series and/or parallel assembly of acoustic elements and was chosen in the current work because of its ease of use in the analysis of simple acoustic resonators. In this method, an acoustic resonator can be represented as a set of interconnected lumped elements using an equivalent circuit that allows obtaining its surface impedance by following an impedance analysis. For this purpose, the acoustic impedances of the elements that make up the resonator must be known beforehand. There exist some basic acoustic elements (eg. acoustic mass, compliance, and resistance) that may serve to in turn describe simple acoustic components such as a narrow tube or an air cavity. The expressions for the acoustic impedances of these components in the linear regime can be easily found in the literature [17, 18].

The acoustic impedance for a uniform circular cross-section tube of finite length t accounting with viscothermal loss mechanisms is given by

$$Z_{TUBE} = j\omega\rho_0 t \left(1 - \frac{2}{s\sqrt{-j}}\frac{J_1\left(s\sqrt{-j}\right)}{J_0\left(s\sqrt{-j}\right)}\right)^{-1} \tag{2}$$

where $s = d(\omega\rho_0/(4\eta))^{1/2}$, being d the diameter of the tube, ω the angular frequency, and η the dynamic viscosity of air; being J_0 and J_1 the Bessel functions of the first kind and zeroth and first order, respectively.

On the other hand, the acoustic impedance of an air cavity of depth l reads

$$Z_{CAVITY} = -jZ_0 \cot\left(k_0 l\right) \tag{3}$$

where $k_0 = \omega/c_0$ is the wavenumber in air.

Hence, the ECM is a simple method for handling simple acoustic systems whose geometrical characteristics can be directly measured, as is the case of the structures to be described next.

3 Materials

3.1 Cellular Material Structures Under Study

Figure 1 shows a schematic representation of the three different types of cellular structures under study (Types A, B, and C), which consist of a bi-dimensional periodic array of spherical cavities of diameter D (pores), and their corresponding unit cells.

While Types A and B were fabricated using an additive manufacturing procedure over polymer material, Type C was prepared using a replication method over metallic material. All structures feature cylindrical openings (pore windows) with diameter d and length t on each side of the pore normal to the bi-dimensional plane, while Types B and C also show cylindrical in-plane interconnections between pores with the same dimensions as the openings except in the case of Type C, whose length may be considered negligible (see Fig. 1c). The pore windows on each side of the pore normal are laterally spaced a distance b, that being $b = D + 2t$ for Types B and C. The materials, of thickness e, were then trimmed to obtain circular cross-section specimens with an average diameter of 29.30 mm to be mounted in the impedance tube.

3.2 Raw Materials

Polymeric cellular materials were manufactured with polyacrylate-based resin provided by Liqcreate (Utrecht, The Netherlands). The metallic cellular material was manufactured using high purity aluminium (99.999 percent) acquired from Alfa Aesar (GmbH & Co KG—Karlsruhe, Germany) and analytical grade sodium chloride particles (99.5 weight percent) purchased from Panreac Química S.L.U. (Barcelona, Spain).

3.3 Additive Manufacturing of Polymeric Cellular Materials

Micro-manufacturing processes offer an excellent workbench for the prototyping and design of sound-absorbing materials [19]. A commercial 3D printer (Autodesk Ember, USA) was used in this work to fabricate the polymeric cellular materials using Projection micro-stereolithography (PμSL) printing technology. Unlike other common additive manufacturing processes such as Fused Deposition Modeling, PμSL technology allows overcoming limitations on the slope of the overhang, which is of great importance in spherical geometries like those under consideration. This technique was successfully used by the

Fig. 1 Schematic representations of the three types of cellular materials under study and their corresponding unit cells: **a** Type A (polymeric material with unconnected pores); **b** Type B (polymeric material with interconnected pores); and **c** Type C (metallic material with interconnected pores). Pore window diameter, d; spherical cavity diameter, D; thickness of the material, e; pore window length, t
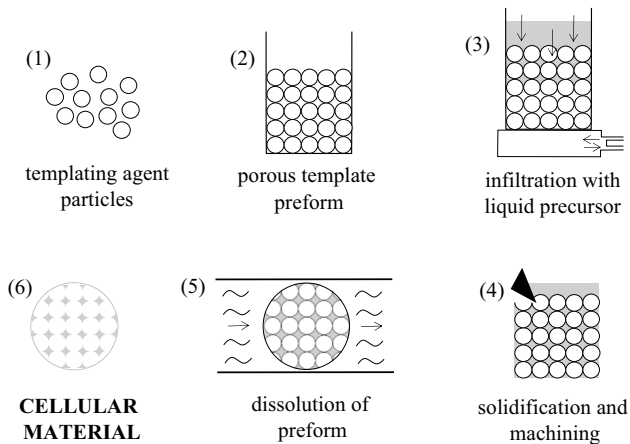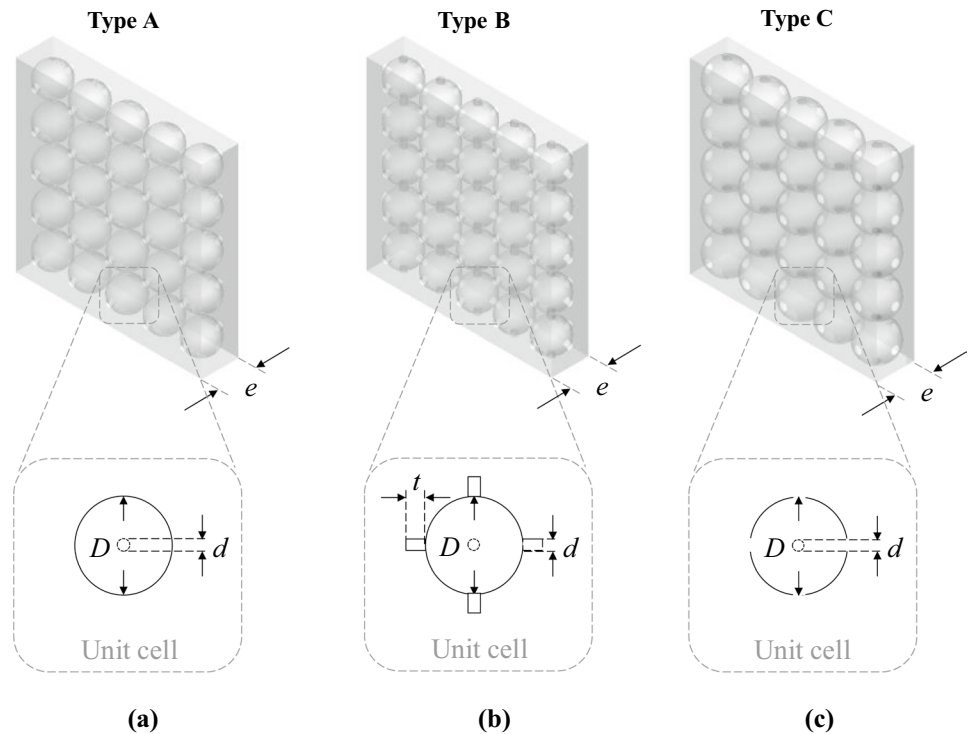
Type A

Type B

Type C

(a)

(b)

(c)

Fig. 2 Steps in the processing of cellular materials by the replication method

authors previously in the fabrication of perforated panels with oblique perforations for sound absorption [20].

## 3.4 Fabrication of Aluminium Cellular Materials

To fabricate the cellular aluminium material (Type C) depicted in Fig. 1c the replication method was followed, which appears to be the most interesting as it allows for proper material control. In this traditional method, schematically represented in Fig. 2, a porous preform, usually of packed particles, is prepared with a templating agent (sodium chloride, carbon, etc.) and then infiltrated with molten metal or any other matrix liquid precursor to produce a composite material. After solidification of the liquid precursor, the preform is removed via dissolution or controlled chemical reaction (eg. by combustion) to leave an interconnected porous structure that can be considered as the "negative" of the initial preform. The versatility of the replication method allows for the control of volume fraction, size, shape, and pore size distribution. With this precise control, the properties of the manufactured cellular materials can be easily adjusted to the desired range. The sections below develop in-depth the processing steps followed to obtain the aluminium cellular materials.

3.4.1 Fabrication of NaCl Spheres Template

The initial stage in fabricating the aluminum cellular materials is to make the spheres that will serve as templates for the cell cavities [21–23]. Due to its simplicity, the method described in the patent [23] for hand-forming NaCl spheres of varying diameters was chosen for this purpose. An initial mixture of NaCl particles 20–38 μm in diameter (Fig. 3a), organic binder (flour), and wetting agent (distilled water) with a mass ratio of 6:2:2 was placed in a vessel. The resulting material was manually shaped into spheres. An average sphere diameter of 5.7–6.7 mm was selected by sieving with standard stainless steel sieves. After being dried at room

Fig. 3 **a** Scanning electron microscopy (SEM) micrograph of NaCl particles of 20–38 µm average diameter and **b** photograph of NaCl spheres prepared by the method described in [19]

(a)   (b)
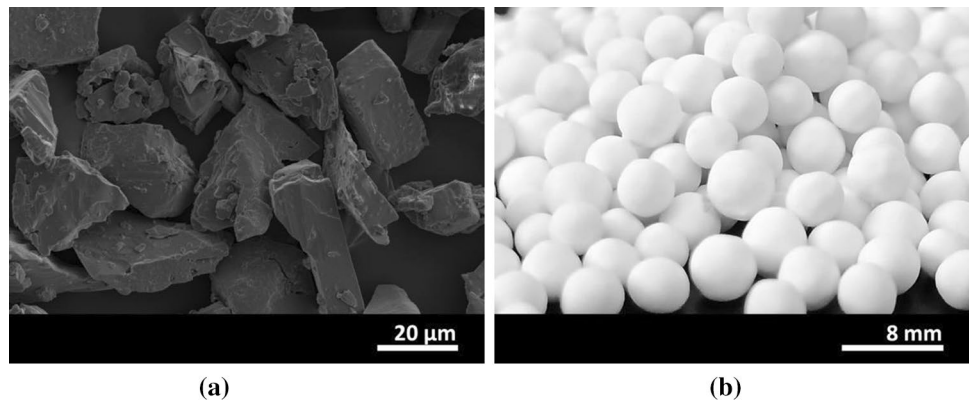
temperature, the spheres were subjected to a two-step heat treatment: (i) carbonization of the organic binder for 60 min at 200 °C, and (ii) oxidation of the residual carbon for 6 h at 500 °C. To avoid structural cracking, both processes were conducted at a heating rate of 4°Cmin^{-1}. Figure 3b illustrates the NaCl spheres produced in this investigation.

3.4.2 Fabrication of Porous Template Preforms

The porous preform was prepared by carefully packing NaCl spheres into a graphite crucible. The packing must permit the spheres to fit into the specified packing structure while maintaining the structural integrity of the particles. The intended packing structure for the spheres is a simple cubic packing, resulting in a solid volume fraction of approximately 0.52. Notably, simple cubic packing does not occur naturally when particles are arranged on top of one another, as particles in the upper layers tend to lodge in the voids left between particles in the lower layers, forming compacts with a volume fraction of 0.60 [24] in random compaction mode (via vibration, for example). Therefore, the simple cubic structure necessary to achieve the desired arrangement of cell cavities must be imposed. For this purpose, graphite crucibles with interior dimensions of $31.0 \times 6.2 \times 31.0$ mm, which are multiples of the average diameters of the spheres (6.2 mm), were considered to accommodate an integer number of 25 spheres in a plane defining planar compaction in which the coordination between spheres is 4.

3.4.3 Obtaining Aluminum Cellular Materials by Infiltration of NaCl Porous Preforms

The preforms were infiltrated with liquid aluminium by pressure-assisted infiltration (see [25, 26] for infiltration of liquid metal into porous preforms formed by the compaction of ceramic particles). For this purpose, a solid piece of aluminium was placed on top of the packed porous preform, and the entire structure was placed in a pressure chamber. The chamber was evacuated to a pressure of 2 mbar before

being heated to 760 °C at a rate of 5 °C min^{-1}. After ten minutes at a steady temperature, the vacuum was released and the chamber was pressurized to 2 bar with argon gas to inject molten metal into the porous preform. The pressurized chamber was then cooled to room temperature by immersion in water to facilitate rapid, directional solidification of the metal. The resulting material was machined into a circular cross-section of 39.30 mm average diameter by grinding with SiC sandpaper of successive grit sizes of 80, 240, 400, and 600 mesh. According to [27], the NaCl preform was subsequently dissolved in water to obtain a metal matrix material with an interconnected porous structure.

4 Methods

4.1 Microstructural Characterization of Cellular Materials

The microstructures of polymeric and metallic cellular materials microstructures were examined using an Olympus PME-3 optical microscope. Image analysis was used to determine the sizes of pore windows, pore window lengths, and spherical cavities. Nevertheless, estimating the cavity diameter in the metallic cellular material is a complicated task since the cavities exposed to the surface of the material are sectioned into different planes and do not represent their true size. Bearing in mind that the replication method reproduces the geometry of the particle template in the cavities (and that the aluminium/NaCl system is non-reactive [23]), an indirect study of the cavity features was performed using image analysis of the NaCl spheres. Their sizes were determined after averaging the maximum and minimum Feret diameters over 100 particle measurements. The same procedure was followed to determine the size of the pore windows in the metallic sample (here, by measuring the exposed windows of the material). Since the NaCl particles in the preform are in touch either at a single point or in a small area due to their relative spherical irregularity, the infiltration

of the metal generates pore window channels of negligible length when compared to the idealized polymeric samples.

Insomuch as most prediction models used to describe the acoustic wave propagation in sound absorbers make use of physical parameters which depend on their microstructure, it was found useful to briefly outline the determination of these parameters for the cellular materials under study. A well-known approach for the description of porous sound absorbent media on a macroscopic scale is the Johnson-Champoux-Allard (JCA) model [28, 29], which relies on the determination of five physical parameters, to list: flow resistivity (σ), tortuosity (α_∞), porosity (ϕ), viscous characteristic length (Λ), and thermal characteristic length (Λ'). Hence, the determination of these so-called non-acoustic properties constitutes a key point to address porous media characterization. In this work, experimental data obtained from microstructural characterization was used to obtain the porosity and the viscous and thermal characteristic lengths of the samples. The remaining parameters (i. e. tortuosity and flow resistivity) were retrieved using an inverse methodology which has become very popular among acousticians [30–32] because of its immediacy and simplicity, its use being of great interest to cope with limitations in laboratory equipment availability, even though special care must be taken on its applicability to guarantee a robust identification procedure [33]. Alternatively, a microstructural analysis like that described in [34] could be used. The inverse methodology herein implemented makes use of the Nelder-Mead direct search optimization method [35] to minimize the difference between the sound absorption coefficient predicted using the JCA model and that measured using the standardized procedure to be described next.

4.2 ASTM E1050 for the Determination of Sound Absorption Coefficient

The ASTM E1050 [36] is a test method for the determination of the sound absorption coefficient of acoustic materials under normal incident plane waves. To this end, the sample to be analysed is placed at the end of an air-filled tube and the sound pressure field is measured with two microphones flush-mounted on it when a speaker positioned on the other end of the tube generates a random noise signal. The surface impedance and sound absorption coefficient of the tested material can be easily calculated by following the so-called transfer function method, which uses the pressure frequency spectrum data at both microphone positions. In this work, the measurement system used to perform the experiments consisted of an impedance tube apparatus BSWA SW470 with an inner diameter of 30 mm, an acquisition card MC3522, a power amplifier PA50, and two 1/4″ microphones type MPA416. The calculation of the surface impedance and the sound absorption coefficient is performed

by the VA-LAB2 software provided by BSWA. It should be noted that the impedance tube rig includes a graded plunger to measure the air gap between the sample and the backing wall (i. e. the cavity that forms the acoustic resonator). Besides, the contour of all the samples was wrapped with very thin tape to avoid undesired air leaks.

5 Results and Discussion

5.1 Geometrical Characterization of the Cellular Materials

Figure 4 shows pictures of the polymeric cellular samples prepared using the PμSL technology and the aluminium cellular material fabricated using the replication method, their average geometrical characteristics summarized in Table 1.

Figure 5a and b show the distributions of window and pore size, respectively, of the manufactured materials. Both plots show very similar values for the type A and type B specimens, with mean deviations at d and D of less than 2.25 and 1.05 percent, respectively. These low error percentages, as well as the fact that the distribution curves are narrow, are the result of the high precision achieved by the PμSL technology used to produce the polymer matrix materials. The metallic sample, on the other hand, has a wider distribution of values and a larger mean pore diameter than the polymeric materials, which is due to the size of the spherical NaCl particles used as templates in the fabrication of the replicable preforms. Similarly, the window sizes are determined by several factors such as the intrinsic properties of the metal in liquid form, the particle diameter, the metal-particle interface, and the pressure at which the metal is infiltrated into the porous preform. The distributions obtained for the distance between windows in polymeric and metallic samples are shown in Fig. 5c. As a result of the processing techniques, these values show similar tendencies as those in Fig. 5a and b.

It should be clarified that the Gaussian curve fitting over experimental values distributions yields an average value of b larger than D, thus involving that the spherical cavities in the case of material Type C are not laterally interconnected, which is not correct and may be attributed to the slight deviation in the fitting procedure.

Once the geometrical characteristics of the samples were measured, the physical parameters that let describe these porous structures on a macroscopic scale were determined. The porosity was determined from the experimental data obtained following the procedure described in Sect. 4.1, whereas the viscous and thermal characteristic lengths were obtained directly from geometrical data in Table 1 given that viscous effects occur mainly in the inter-connection between the spherical cavities [28] and the thermal effects

Fig. 4 Photographs of the fabricated cellular materials: **a** Type A (polymeric material with unconnected spherical cavities), **b** Type B (polymeric material with interconnected spherical cavities), and **c** Type C (metallic material with interconnected spherical cavities)
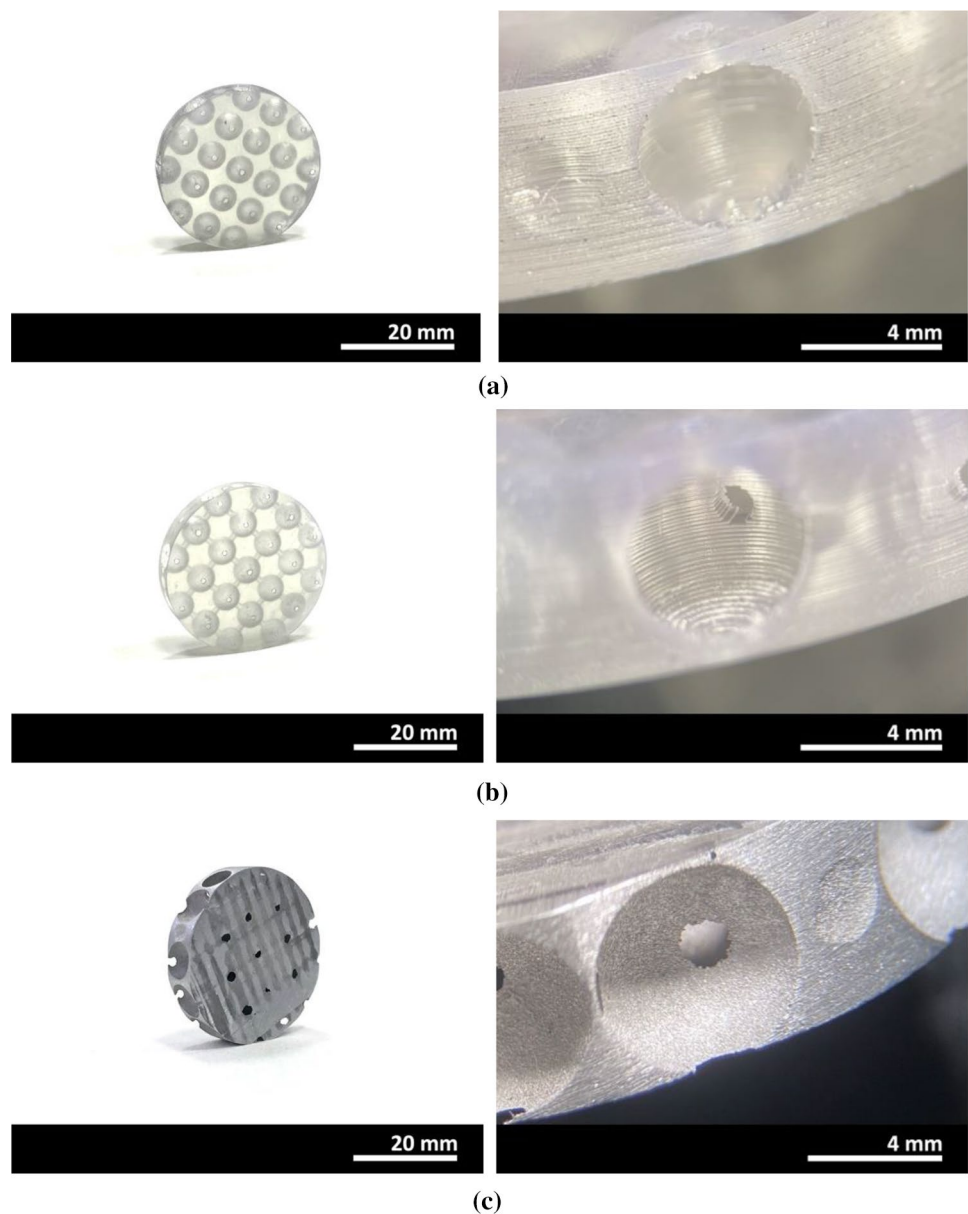

(a)

(b)

(c)

Table 1 Average design geometrical characteristics of the fabricated cellular materials

Cellular structure	b (mm)	d (mm)	D (mm)	e (mm)	t (mm)[*]
Type A	5.82	0.92	4.90	5.77	0.436
Type B	5.84	0.90	4.85	5.81	0.478
Type C	6.26	1.16	6.20	6.11	–

[*]Obtained indirectly from measured parameters D and e

are related to the largest size of the pores [29]. The remaining parameters were retrieved using the inverse methodology described in Sect. 4.1 with a relative error lower than 6.5% (tortuosity and flow resistivity) and from the direct relation $\sigma = \eta/q_0$, where q_0 stands for the static permeability. Table 2

summarizes the results obtained for the different cellular structures under study.

Results indicate that the polymeric samples fabricated using additive manufacturing technology show lower porosities and higher tortuosity values than the metallic samples, which results in a lower frequency resonance peak when used as a part of a resonator system, as it will be shown in Sect. 5.3. As for the flow resistivity and permeability values, the polymeric samples showed higher (lower) values and consequently a higher sound absorption (see Sect. 5.3), which may be also attributed to the smaller characteristic lengths that describe the microstructure of the materials. Even though the above parameters could be used in the JCA model to study the acoustic behaviour of the materials under study by using the corresponding expressions for the
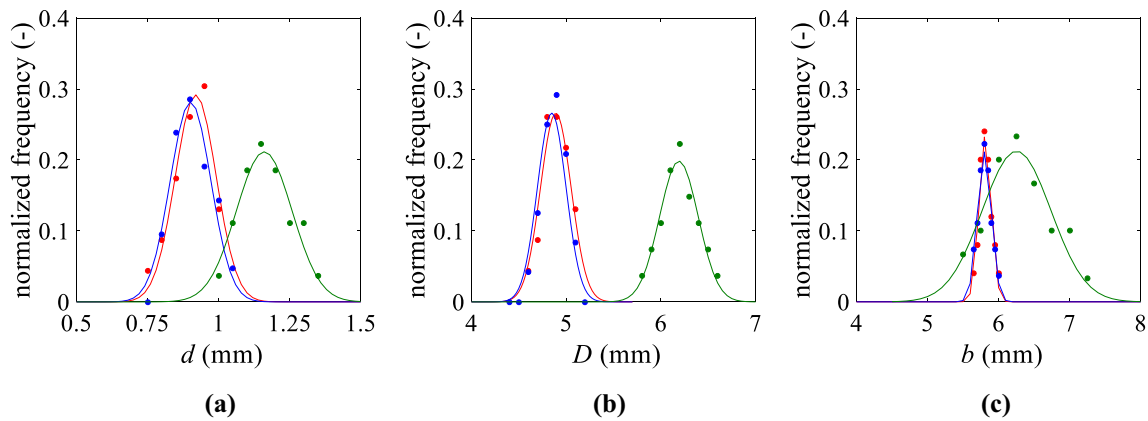
Fig. 5 Measured (markers) and Gaussian fit (lines) of the fabricated cellular material structures (Type A: red; Type B: blue; and Type C: Green): **a** pore window diameter, d; **b** spherical cavity diameter, D; and **c** lateral distance between pore windows, b

Table 2 Macroscopic parameters of the fabricated cellular materials

Cellular structure	α_∞^* (-)	Λ (μm)	Λ' (μm)	ϕ (-)	σ^* (Ns/m⁴)	q_0 (m²)
Type A	7.1	460	2450	0.34	54441	$3.18 \cdot 10^{-10}$
Type B	8.6	450	2425	0.35	116740	$1.57 \cdot 10^{-10}$
Type C	5.3	580	3100	0.56	32979	$5.55 \cdot 10^{-10}$

*Obtained using an inverse methodology
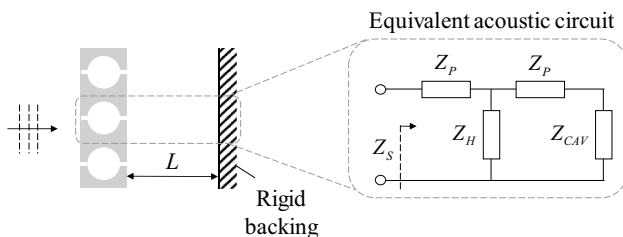
Fig. 6 Schematic representation of the acoustic resonator system and the proposed equivalent acoustic circuit

complex dynamic density [28] and bulk modulus [29], a simplified approach based on the ECM was chosen instead as it will be described next.

5.2 Proposed Approach for the Modeling of the Cellular Structures

In what follows, a prediction approach to obtain the surface impedance of the acoustic resonator systems under study using the ECM is outlined. For this purpose, a description of the absorber in terms of its acoustic components is first given. From visual inspection of Fig. 1, the unit cells of the cellular material structures can be described in a simplified way as two short cylindrical tubes coupled through a large spherical cavity. Besides, the rear face of the materials is in turn coupled to the backing air cavity of the resonator by

one of these tubes. Figure 6 shows a schematic representation of the resonant system under analysis and the proposed equivalent acoustic circuit for a unit cell of the absorber.

In that circuit, the acoustic impedance Z_P corresponds to the inlet/outlet tubes (i. e. the pore windows), Z_H to the spherical cavity of depth D, and Z_{CAV} to the backing air cavity of depth L. Besides, to account for the inertial effect and the viscous dissipation at the inlet/outlet of the pore windows, a reactance term, and a resistance term must be added to the acoustic impedance of each tube such that

$$Z_P = Z_{TUBE} + \delta 2R_S + j\omega\rho_0 0.85d \tag{4}$$

being δ a factor that accounts for the pore window type ($\delta = 4$ for sharp-edged case) and $R_S = (\eta\rho_0\omega/2)^{1/2}$ the surface resistance, which is accounted twice for each pore window as energy dissipation occurs when the flow enters and exits the tube [13]. Note that additional branches would be necessary for that circuit to account for the pore windows interconnecting the spheres with each other, herein not being considered for the shake of simplicity although these may have a slight influence on the tortuosity of the cellular structure as confirmed in the experimental data to be presented in Sect. 5.3.

Once the acoustic components that make up the acoustic resonator were identified, their respective acoustic impedances can be directly calculated by substitution of the corresponding geometrical characteristics of Table 1 in Eqs. (2) and (3) provided the backing air cavity depth L is also set. It

must be noted that Eq. (2) was used for the narrow cylindrical pores (i. e. the pore windows) while Eq. (3) was used for the air cavities with $l=L$ for the backing air cavity (Z_{CAV}) and $l=0.806D$ for the spherical cavities (Z_H) as proposed in [13]. Thereby, after some basic circuit theory analysis, the surface impedance under plane wave incidence of the whole absorber (i. e. cellular material structure and backing cavity) can be written as follows

$$Z_S = Z_P/\phi + \frac{Z_H\left(Z_P/\phi + Z_{CAV}\right)}{Z_H + Z_P/\phi + Z_{CAV}} \qquad (5)$$

where $\phi = \pi(d/2)^2/b^2$ is the open area ratio necessary to account for the fraction of pore open area on the front/rear face of the material, being b the lateral distance between pore windows [17]. Finally, by substitution of the surface impedance calculated with Eq. (5) in Eq. (1) the sound absorption coefficient of the acoustic resonator can be obtained.

5.3 Sound Absorption Results

Predictions of the sound absorption performance of the different cellular material structures under study were performed by using the measured geometrical characteristics of the fabricated specimens and the proposed modeling approach previously described. Additionally, the fabricated samples were mounted in the impedance tube and their sound absorption coefficient was measured by following the procedure described in the standard ASTM E1050. Furthermore, to confirm the tuning capabilities of these materials when used as resonator systems, different air cavity depths L in the range from 5 to 30 mm were tested both in the predictions and the experiments. Figure 7 shows a comparison of the measured and predicted sound absorption coefficient of the analysed materials for different values of L.

In general, results show both the good sound absorption performance of the analysed cellular structures in addition to their tuning capabilities, being the resonance peaks shifted from around 2000 Hz in the polymeric samples (2700 Hz in the metallic one) for an air cavity depth of 5 mm to down below 800 Hz (1200 Hz in the metallic one) for an air cavity depth of 30 mm. On the other hand, predicted sound absorption shows a good agreement when compared to the experiments, the discrepancies in the case of the metallic material (Type C) being attributed to a higher variance in its geometrical characteristics when compared to additively manufactured ones (see Fig. 5) which results in an overestimation of the peak absorption amplitudes, these being more significant as the air cavity depth increases. In this regard, the factor δ can be fitted to be frequency-dependent and account for the non-sharp edge following a procedure similar to that described in [36]. It should be also recalled that the pores connecting
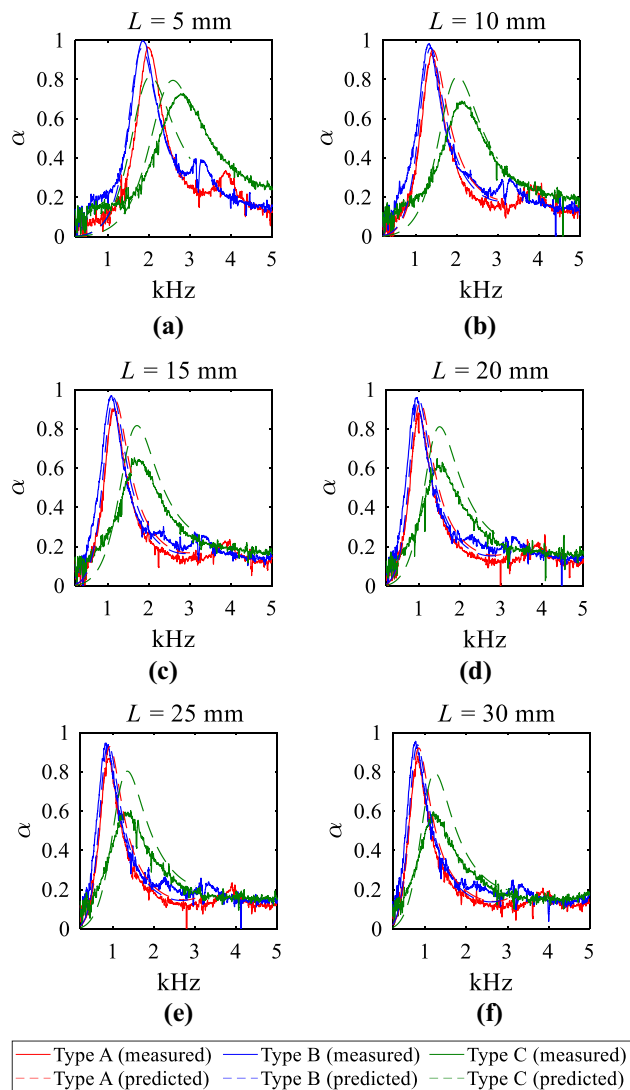

Fig. 7 Comparison of the predicted (discontinuous lines) and measured (continuous lines) sound absorption coefficient spectrum of the cellular material structures (Type A: red; Type B: blue; Type C: green) for different air cavity depths L: **a** 5 mm, **b** 10 mm, **c** 15 mm, **d** 20 mm, **e** 25 mm, and **f** 30 mm

the spheres were not taken into account in the proposed approach because this effect was considered negligible in the frequency range of analysis for the geometrical characteristics of the material, further research on this point is worth investigating in the future. Also, note that in all cases the baffle conditions in the impedance tube setup differ from the infinite lateral extend commonly assumed in most prediction models [17]. Moreover, unlike statistical methods for predicting sound-absorbing properties of stochastic porous metal materials as that presented in [37], the proposed approach can be used for cellular materials with a specific non-stochastic structure. All the same, the above results verify the usefulness of this approach for

the modeling and design of cellular material structures in a simple manner.

To further analyse the sound absorption performance of the fabricated materials, several sound absorption indicators were calculated from the experimental curves depicted in Fig. 7, specifically the Noise Reduction Coefficient (NRC), the Sound Absorption Average (SAA), the Half-bandwidth (HBW), and the resonance frequency peak amplitude (α_{peak}). These parameters were shown to be very useful to compare the impact of different microcellular structures on the sound absorption spectra for automotive exhaust performance mufflers [38]. The sound absorption indicators of the three cellular structures for the different resonator configurations under study are listed in Table 3.

Results indicate that cellular structure Type B shows higher NRC and SAA values when compared to the other structures for most resonator configurations under study, which may be attributed to the extra dissipation mechanisms occurring in the lateral interconnection tubes between spherical cavities. It should be noted that the SAA improves as the air cavity depth increases, which highlights the potential of these structures to be used as acoustic resonators in practical applications as will be discussed in Sect. 5.5. On the other hand, the cellular structure Type C show a higher HBW than the polymeric samples due to the higher porosity values and larger pore windows and spherical cavities. Conversely, the resonance frequency peak amplitude is lower in the case of the metallic sample whereas it almost reaches perfect absorption in the polymeric ones.

Table 3 Sound absorption indicators of the fabricated cellular materials

| L (mm)	Cellular structure	NRC	SAA	HBW (Hz)	α_{peak}
5	Type A	0.38	0.30	840	0.97
	Type B	0.40	0.38	928	1.00
	Type C	0.21	0.25	2060	0.73
10	Type A	0.25	0.35	746	0.93
	Type B	0.35	0.44	798	0.98
	Type C	0.33	0.32	1790	0.69
15	Type A	0.37	0.38	716	0.91
	Type B	0.46	0.46	762	0.97
	Type C	0.32	0.33	1520	0.65
20	Type A	0.40	0.39	698	0.88
	Type B	0.46	0.47	760	0.96
	Type C	0.30	0.34	1434	0.65
25	Type A	0.39	0.41	654	0.87
	Type B	0.45	0.49	718	0.95
	Type C	0.31	0.35	1596	0.60
30	Type A	0.38	0.42	640	0.88
	Type B	0.44	0.49	694	0.96
	Type C	0.32	0.35	1350	0.60

5.4 Parametric Study

The above results both confirm the good sound absorption performance of the cellular material structures and the utility of the different techniques in the fabrication of such structures. However, the resulting porous media may still exhibit enhanced sound absorption features if its microstructure is properly designed. To confirm this assertion, a parametric study of the sound absorption performance of the material in terms of its geometrical characteristics was carried out by using the derived model. The influence of both the diameter of the pore windows and the diameter of the spherical cavities was analysed. In doing so, the average sound absorption coefficient (α_{avg}) over the frequency range between 500 and 5000 Hz was calculated for pore window and sphere diameters ranging from 0.1 to 0.5 mm and 0.5 to 5 mm, respectively. The remaining geometrical parameters were kept constant with values of $t = 0.5$ mm for the pore window length and $L = 5$ mm for the backing air cavity depth, being the lateral distance between pores equal to the diameter of the spherical cavities (i. e. $b = D$). Figure 8a shows the predicted average sound absorption coefficient resulting from varying the corresponding geometrical parameters.

Results show that maximum sound absorption can be reached for a pore window size of 0.18 mm and a sphere diameter of 0.8 mm (white circle). In Fig. 8b, a more detailed analysis of the corresponding sound absorption coefficient curve reveals that the "optimum" case outperforms the ones analysed in Sect. 5.3, especially in the mid-high frequency range. It should be mentioned that the pore window length and the air cavity depth could also be modified, the expected effect when these are reduced being a shift of the resonance peak towards lower frequencies [39]. This feature turns out of great utility for such applications requiring tuning the resonance in a specific target frequency as will be discussed next.

5.5 Remarks on the Potential Applications of Cellular Material Structures

Even though the main objective of this work was to investigate the sound absorption performance of cellular material structures fabricated using different techniques, it was also considered of great interest to highlight the wide range of acoustic applications for this type of material. Some examples of this particular metamaterial structure in the field of acoustics are the design of modular acoustic filters for musical wind instrument prototyping [40] or automotive silencers for sound attenuation [41]. Given the metallic nature of the fabricated materials, these may become a valuable alternative to conventional additive manufacturing processes because of the higher durability and robustness required normally in the validation

Fig. 8 a Contour map of the predicted average sound absorption coefficient α_{avg} for a resonator system with $L=5$ mm over the frequency range between 500 and 5000 Hz as a function of the diameter of the pore windows, d, and the diameter of the spherical cavities, D. **b** Sound absorption coefficient curve of the reference configuration (see results for Type C in Fig. 7a) versus the "optimized" configuration obtained in the parametric study ($d=0.18$ mm, $D=0.8$ mm)

(a)

(b)
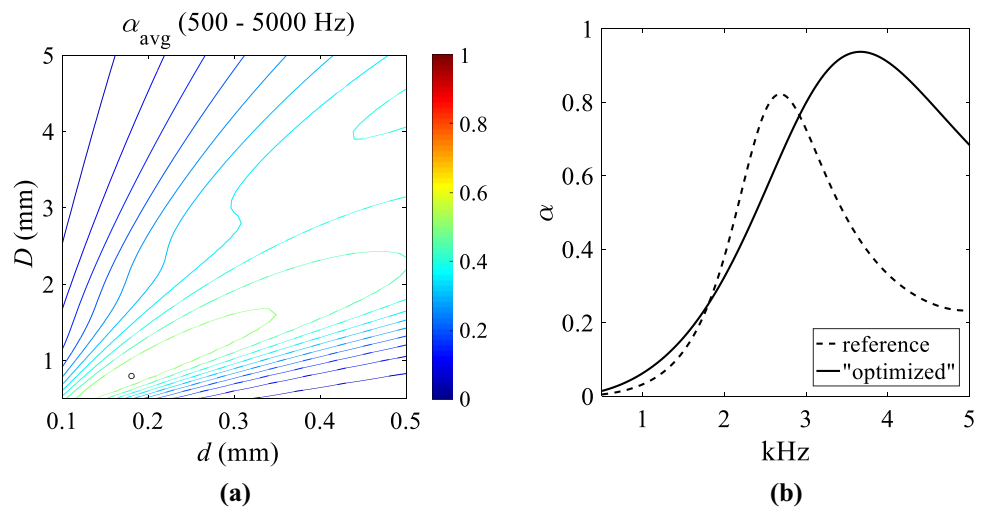
stage of industrial product fabrication. Moreover, these materials could be also conceived under severe conditions such as for noise reduction during the launch of rockets [42]. Obviously, these are far from easy tasks and much research would be needed, but the fire resistance features of the fabricated materials make it an excellent candidate when compared to conventional porous media and further encourages this research.

6 Conclusions

An open-pore aluminium cellular material with a non-stochastic structure was designed to yield a resonant system for sound absorption. An equivalent acoustic circuit of such a system was derived by using the Equivalent Circuit Method (ECM) and verified experimentally by measuring the sound absorption coefficient following the procedure described in the ASTM E1050. The effect of the air cavity depth on its sound absorption performance was also evaluated both theoretically and experimentally, being the resonance peak shifted towards lower frequencies as the cavity depth increases. Finally, it was theoretically shown that the average sound absorption coefficient of these cellular structures can be further improved within the frequency range between 500 and 5000 Hz by appropriately selecting the design characteristics of the non-stochastic structure, specifically the diameters of the pore windows and spherical cavities. Compared to other conventional sound-absorbing materials, the proposed material is expected to maintain its sound-absorbing properties in extreme conditions (eg. high temperature). Overall, preliminary results demonstrate the potential of these materials as sound absorbers and encourage further research on their development for noise reduction applications.

Declarations

Conflict of interest The authors declare that they have no known competing financial interests or personal relationships that could have appeared to influence the work reported in this paper.

References

1. J. Cao, Q. Fu, Y. Si, B. Ding, J. Yu, Compos, Commun, **10**, 25 (2018)
2. W. Zhai, X. Yu, X. Song, L.Y.L. Ang, F. Cui, H.P. Lee, T. Li, Mater. Design **137**, 108 (2018)

3. A.J. Otaru, Met. Mater. Int. **26**, 915 (2020)
4. T.J. Lu, A. Hess, M.F. Ashby, Appl. Phys. **85**, 7528 (1999)
5. A.J. Otaru, H.P. Morvan, A.R. Kennedy, Scripta Mater. **150**, 152 (2018)
6. T.J. Lu, A. Hess, M.F. Ashby, J. Appl. Phys. **85**, 7528 (1999)
7. C. Perrot, R. Panneton, X. Olny, J. Appl. Phys. **101**, 113538 (2007)
8. F. Chevillotte, C. Perrot, R. Panneton, J. Acoust. Soc. Am. **128**, 1766 (2010)
9. K.C. Opiela, T.G. Zieliński, T. Dvorák, S. Kúdela Jr., Appl. Acoust. **174**, 107706 (2021)
10. S. Deshmukh, H. Ronge, S. Ramamoorhy, Mater. Design **175**, 107830 (2019)
11. N. Jimenez, W. Huang, V. Romero-García, V. Pagneux, J.-P. Groby, Appl. Phys. Lett. **109**, 121902 (2016)
12. C. Claeys, E. Deckers, B. Pluymers, W. Desmet, Mech. Syst. Signal Pr. **70–71**, 853 (2016)
13. L.-W. Cheng, C.-W. Cheng, K.-C. Chung, T.-Y. Kam, Appl. Phys. A **123**, 37 (2017)
14. J. Kennedy, L. Flanagan, L. Dowling, G.J. Bennett, H. Rice, D. Trimble, Int. J. Polym. Sci. **2019**, 7029143 (2019)
15. A. Seçgin, T. Baygün, Mater. Res. Express **6**, 065801 (2019)
16. R. Sailesh, L. Yuvaraj, M. Doddamani, L.B. Mailan Chinnapandi, J. Pitchaimani, Appl. Acoust. **186**, 108457 (2022)
17. J.F. Allard, N. Atalla, *Propagation of Sound in Porous Media: Modelling Sound Absorbing Materials*, 2nd. edn (John Wiley and Sons, Chichester, 2009)
18. L. Beranek, T. Mellow, *Acoustics: Sound Fields and Transducers* (Academic Press, Waltham, 2012)
19. T. Zieliński, K.C. Opiela, P. Pawłowski, N. Dauchez, T. Boutin, J. Kennedy, D. Trimble, H. Rice, B. Van Damme, G. Hannema, R. Wróbel, S. Kim, S. Ghaffari Mosanenzadeh, N.X. Fang, J. Yang, B.B. de La Hosseraye, M.C.J. Hornikx, E. Salze, M.-A. Galland, R. Boonen, A.C. de Sousa, E. Deckers, M. Gaborit, J.P. Groby, Addit. Manuf. **36**, 101564 (2020)
20. J. Carbajo, S. Ghaffari Mosanenzadeh, S. Kim, N.X. Fang, Appl. Phys. Lett. **116**, 054101 (2020)
21. A. Jinnapat, A.R. Kennedy, J. Alloy. Compd. **499**, 43 (2010)
22. R. Goodall, A. Mortensen, Adv. Eng. Mater. **9**, 951 (2007)
23. A. Mortensen, A.R. Goodall, Method of producing a porous metallic article, European Patent EP2118328B1 (2011)
24. F.Ç. Durmus, L.P. Maiorano, J.M. Molina, Int. J. Heat Mass Transf. **191**, 122852 (2022)
25. J.M. Molina, R.A. Saravanan, R. Arpón, C. García-Cordovilla, E. Louis, J. Narciso, Acta. Mater. **50**, 247 (2002)
26. J.M. Molina, E. Piñero, J. Narciso, C. García-Cordovilla, E. Louis, Curr. Opin. Solid State Mater. Sci. **9**, 202 (2005)
27. L.P. Maiorano, J.M. Molina, Mater. Design **158**, 160 (2018)
28. D.L. Johnson, J. Koplik, R. Dashen, J. Fluid Mech. **176**, 379 (1987)
29. Y. Champoux, J.F. Allard, J. Appl. Phys. **70**, 1975 (1991)
30. M. Vašina, D.C. Hughes, K.V. Horoshenkov, L. Lapčik, Appl. Acoust. **67**, 787 (2006)
31. A. Geslain, J.P. Groby, O. Dazel, S. Mahasaranon, K.V. Horoshenkov, A. Khan, J. Acoust. Soc. Am. **132**, 208 (2012)
32. J. Ramis, R. Del Rey, J. Alba, L. Godinho, J. Carbajo, Mater. Construcc. **64**, e008 (2014)
33. T.G. Zieliński, J. Acoust. Soc. Am. **137**, 3232 (2015)
34. J.A. Nelder, R. Mead, Comput. J. **7**, 308 (1965)
35. ASTM E1050, Standard Test method for impedance and absorption of acoustic materials using a tube, two microphones and a digital frequency analysis system (ASTM International, West Conshohocken, 2012)
36. T. Herdtle, J.S. Bolton, N.N. Kim, J.H. Alexander, R.W. Gerdes, J. Acoust. Soc. Am. **134**, 4752 (2013)
37. D. Guan, J.H. Wu, L. Jing, J. Alloy. Compd. **626**, 29 (2015)
38. A.J. Otaru, O.E. Odumu, Z. Manko, A.G. Isah, R.O. Isa, M.R. Corfield, Appl. Acoust. **187**, 108508 (2022)
39. U. Ingard, J. Acoust. Soc. Am. **25**, 1037 (1953)
40. D. Li, D.I.W. Levin, W. Matusik, C. Zheng, ACM T. Graphic. **35**, 88 (2016)
41. D. Deery, J. Kennedy, Vibroeng. Proc. **37**, 66 (2021)
42. I. Herrero-Durá, Acoustic noise reduction methods for launch pad, Ph. D. Thesis, Valencia Polytechnic University (2020)